Observation of mass transport stability and Faraday instability: why stable single bubble sonoluminescence is possible

R. Glynn Holt and D. Felipe Gaitan

(Jet *Propulsion Laboratory, California Institute of Technology, Pasadena, CA 91109)*

Abstract

The region of parameter space (acoustic pressure} P_a, bubble radius R_0) in which stable single bubble sonoluminescence (S1]S1.) occurs in an air-water system is a small fraction of that which is accessible. This is due to the existence of an island of dissolution at high P_a and small R_0. For dissolved gas concentrations above 50% of saturation, the region lies above the threshold for shape oscillations, and is unobservable. Below S()%, an oscillating bubble is stabilized on the boundary of the island which lies below the shape threshold. SBSL is shown to exist exclusively along this boundary. [PACS: 43.25.Y,47.55.Bx,42.65.Re,47.52.+j]

observation of mass transport stability and Faraday instability: why stable single bubble sonoluminescence is possible

Introduction

A bubble in an external acoustic field is a laboratory for the study of a surprising variety of physics problems. Heat transport [1], mass transport [2], surfactant effects [3], shock waves [4], chaos [5], free surface instability [6], and even electromagnetic radiation [7] are all phenomena associated with the highly nonlinear oscillations of air bubbles in water. Recent observations of *stable single bubble sonoluminescence* (SBSL) have highlighted the fact that, despite the enormous amount of energy concentrated in a bubble which is emitting light, such a bubble can remain both *spherically symmetric* and the *same size* over billions of oscillation cycles!

On the other hand, this behavior is far from typical. Given reasonable initial values for the pressure and frequency of the driving acoustics, bubble size, and host liquid parameters, a bubble is far more likely to dissolve and eventually disappear, or to grow and break up. Although for some cases the growth is self-limiting (see below), most of the time spherical instability will occur, and the bubble will either break up (and sometimes also disappear), or will become so large that it cannot be levitated. in fact, as discovered recently by Löfstedt et al. [2], stable single bubble sonoluminescence is known to occur where classical theories [2,6] predict rapid growth and subsequent destruction! The experiments described in this report represent an attempt to resolve the discrepancies between observation and model predictions. In particular, we wish to delineate where and how a bubble can exhibit both mass transport and mechanical stability by measuring where the instabilities occur for the limiting case of small bubble sizes and large acoustic pressures.

The natural parameter space for the problem is defined by the acoustic pressure P_a and the equilibrium radius R_0. The accessible range for an acoustic standing wave levitator is the minimum trapping pressure (less than 0.1 bar in 1 g, 0 in 0g) up to about 1.5 bars. Bubbles can be stably levitated with radii ranging from less than 1 micron up to approximately 110 microns near the pressure maximum of the 20 kHz standing wave. And yet SBSL is observed only in a minuscule region of that space, which we loosely term the *SL* window: $1.2 \leq P_a \leq 1.4$ bars, and (less than 1) $\leq R_0 \leq 7$ microns in the current measurements at a fixed acoustic driving frequency f_a of 20.6 kHz [8].

We have discovered why this region is so small: in fact, for a fixed concentration of dissolved gas in the liquid, the locus of (P_a, R_0) points where S11S1, occurs forms a *line path* in the space. Asymptotically stable, purely spherical bubble oscillations can occur only if they are in *mass flux equilibrium*, and then only if that equilibrium is itself stable. As we will demonstrate below, these constraints are met when the gas concentration in the liquid is below a certain value: for air in water at room temperature that threshold value is approximately 50% saturation, or equilibration at 380mmHg, corresponding to $C_i/C_0 = 0.5$, where C_i is the dissolved gas concentration in the liquid far away from the bubble, and C_0 is the concentration at equilibrium for an ambient pressure of 1 bar.

For $C_i/C_0 > 0.5$, bubbles arc observed to obey the predictions of the Eller-Flynn [2] diffusion theory, for which Fig. 1 a is representative. Bubbles with initial states (P_a, R_0) in the dark shaded region labeled 'd' dissolve; bubbles in 'g' grow until their oscillation meets the conditions for onset of resonant, parametric (Faraday, [9]) shape oscillations [Holt et al. in 5; Strube, Hullin anti Brenner et al. in 6], where they are no longer spherically symmetric, This shape oscillation threshold is shown in Fig. 1 a-c as the points labeled 'F'. At near-SL acoustic pressures (0.8 - 1.4 bar), these shape oscillations lead to breakup of the bubble. We call this repeated growth, shape oscillation and breakup process *recycling*: to the naked eye it appears as a 'dancing' or 'jittering' motion as reported by numerous authors [10].

For $C_i/C_0 \leq 0.5$, an isolated *island of dissolution is* observed to emerge at smaller R_0 than the Faraday threshold and stabilize the recycling. In Fig. 1 a ($C_i/C_0 = 0.5$) the island just intersects F at (1.2 bar, 7 microns); only this bubble is spherically stable, and light emission begins precisely here. At increasingly lower gas concentrations (Figs. 1b, 1c), this island extends to lower R_0, and covers a larger range of P_a at its intersection with the Faraday threshold. Bubbles (emitting light or not) arc observed to be in *stable* mass flux equilibrium on the boundary of this island. Stable equilibrium requires that a bubble move from a growth regime to a dissolution regime as R_0 is increasing, and vice-versa, Thus the left side of the boundary is a growth region, and the right side is a dissolution region.

SL occurs in bubbles on this boundary, and onl y bubbles on this boundary satisfy the condition for SBSL. However, this stable mass equilibrat ion is a *sufficient* but *not necessary* condition for light emission. For example, in Fig. 1c light is first emitted at the point on the upper segment of the boundary marked by the arrow. No light is emitted by the mechanically and mass flux stable bubbles on the lower segment. Light is observed for recycling bubbles cent inuously along the boundary F for $1.26< P_a \leq 1.4$ in Fig. 1 a [11]. Recycling bubbles are clearly not in dynamic mass equilibrium, diffusive or otherwise, nor are they in mechanical Equilibrium. Thus the light emission mechanism is not slaved to the mechanism for mass equilibration. The importance of the dissolution island is in providing a stable path into an area of parameter space not otherwise accessible (except transiently), and making stable *synchronous* SL possible. Our observations for the more highl y degassed water (Fig. 1 c) fits very well with the observations of the UCLA group [12].

These represent the main observations we wish to report here. The remainder of the paper is devoted to explaining how we made our measurements and the necessary analysis to justify the interpretations presented here.

Description of the measurements and techniques

Air bubbles initiated via electrolysis arc acoustically levitated in water in the 20 khz standing wave field of a cylindrical resonance cell [14]. The acoustic pressure P_a at the antinode is obtained from a custom hydrophone mounted at the z anti node and 1 cm away from the side wall inside the cell. R_0, R_{max} and R_{min} are obtained from single frame video images illuminated at 1 pulse per frame (maximum 1 μs pulse width); R_0 in particular is obtained by turning the sound field off instantaneously. $R(t)$ is obtained from a PMT located at 80° from the forward [15]. Dissolved gas concentrations less than saturation are obtained by allowing the water to equilibrate at a reduced pressure; C_i/C_0 is inferred using Henry's law.

We report here only those measurements for $R_0 \leq$ **20** microns, and $P_a \geq 0.6$ bar, and restrict ourselves to dissolved gas content $0.1 \leq C_i/C_0 \leq 0.5$ [16]. For these conditions, as the acoustic pressure P_a is increased we encounter two (P_a, R_0) parameter regimes where bubbles are in mass flux equilibrium for a fixed C_i/C_0: one usually unstable (corresponding to Eller-Flynn diffusional equilibrium [21), the other stable (the dissolution island boundary). It is practical to measure the point at which the. *unstable* mass equilibrium and the threshold for onset of shape oscillations intersect. Continuing for a fixed concentration, we then increase P_a, and the bubble remains near F because it is recycling. At $P_a = 1.2$ bar, wc encounter the *stable* mass equilibrium regime: the lower boundary of the dissolution island. increasing P_a, wc measure spherically symmetric bubble oscillations along this asymptotically stable boundary, which takes us rapidly to smaller R_0, then back again, scc Fig. 1 b for example. P_a is increased until F is reached again, or the bubble disappears, or both. Wc repeat the process for the next gas concentration value.

Faraday Instability

Only the spherically symmetric volume mode is directly forced by the time-varying acoustic pressure. Under what conditions will this spherical symmetry become unstable, and lead to observable distortions of the shape and eventual breakup of the bubble.?

Our observations show that, for all P_a below the maximum trapping pressure, the instabilit y which develops first is the Faraday instability. Figure 1 shows the measured threshold as a series of points labeled 'F n', that is, the onset of normal shape modal oscillations of observed mode n. The crucial observation which distinguishes this instability from the Rayleigh-Taylor instability [13] is that the normal mode couples resonantly to the nearly periodic ringing oscillation. Thus wc scc the shape mode and concomitant breakup occur 2 or more collapses *after* the first (light-producing) collapse. Brenner et al [6] have presented dc.tailed calculations of the onset of only the quadrupole mode nonlinearly coupled to the volume mode. The numerically generated threshold agrees very well with our measurements until below 8 microns. The internal resonance condition $f_n : f_0 = 1:2$ (where f_n is the lamb [17] frequency for the observed mode and liquid parameters, and f_0 is the linear volume mode resonance frequency) determines the mode we observe.

Mass flux equilibrium: observations, mechanisms, stability

Our observations show that in the subspace of purely spherical oscillations (to the left of F), there exist two apparently disconnected regions of dissolution for $0.2 < C_i/C_0 \leq 0.5$. These regions are denoted by dark shading and labeled as 'd' in Fig. 1a-c. The rest of the accessible space is labeled 'g' for growth. Thus we observe two disconnected sets of dynamic mass equilibria at the boundaries of these regions. The lower equilibrium is unstable, and we only mike measurements where it intersects F; the upper equilibrium is stable, and we can measure the line path of the boundary extending to small R_0 away from F.

Eller and Flynn [2] showed that the net effect of oscillations was to enhance *diffusive* transport of dissolved gas into the bubble. For large enough amplitude oscillations for a fixed C_i, this "rectified diffusion" could dominate the natural dissolution of a bubble in an undersaturated solution. The curves EF in Fig. 1 a - 1 c represent numerical y generated (P_a, R_0) values where an oscillating bubble is in diffusion equilibrium for the same fixed C_i/C_0 as presented in the experimental data, using R(t) calculate.d from a Rayleigh-Plesset model [18]. The dynamic d iffusion equilibrium they derive is

$$\frac{C_i}{C_0} = \left(1 + \frac{2\sigma}{R_0 P_\infty}\right)\frac{\left\langle \frac{R}{R_0} \right\rangle}{\left\langle \left(\frac{R}{R_0}\right)^4 \right\rangle} \qquad (1),$$

where σ is the liquid surface tension, P_∞ is the ambient pressure outside the liquid, and < ... > denotes the time average of the quantity over one acoustic cycle. For example, in Fig. 1 a EF (0.5) represents the condition $C_i/C_0 = 0.5$. For the region (P_a, R_0) above and to the right of EF the model predicts diffusive growth; below left it predicts dissolution. The wiggles in the curve EF (0.5) in Fig. 1a are due to underlying harmonic saddle-node resonances [19]. EF curves with positive slope are stable equilibria -- negative slopes are unstable. Brenner et al. [2] have suggested that the intermittent stable regions such as seen on EF (0.5) in Fig. 1a could be responsible for stable SL; while in practice resonances are important at larger bubble sizes [14, 16], our measurements show that volume resonance effects are not important in the SL window.

EF intersects F very near where our unstable mass equilibrium intersects F in Fig. 1a - 1c, indicating that our unstable mass equilibria result from a diffusive mechanism. However, EF predicts a single connected mass equilibrium line, with a continuous region of growth above and to the right. The Eller-Flynn theory fails to predict our observations of stable mass flux equilibria in the SL window.

We can substitute our measured bubble response R(t) into (1) to further investigate the nature of the equilibria, Table 1 lists the results $C_i/C_{0\,(eq.\,(1))}$ for bubbles at the EF - F intersection for different dissolved gas concentrations $C_i/C_{0\,(meas.)}$. Bubbles at this unstable equilibrium yield very nearly the same C_i as we measure for the liquid. We conclude that these bubbles are in boundary-layer diffusive mass equilibrium, and the Eller-Flynn theory is a valid predictor of such diffusive equilibria. Bubbles at the stable equilibrium along the island boundary exhibit very different values, all of which are at least an order of magnitude smaller than our measured C_i/C_0. Thus such bubbles are not in diffusive equilibrium with air. This is in agreement with the observations of Barber et al. [8] and Löfstedt et al. [2]; they report an air bubble with roughly the same P_a, R_0, R_{max} which does not satisfy an approximate expression derived from (1). As the UCLA group concludes, it seems likely that some other (perhaps non-diffusive) mechanism is responsible for the mass transport here.

Figure 2 plots $C_i/C_{0\,(eq.\,(1))}$ for every bubble in mass flux equilibrium for two similar $C_i/C_{0\,(meas.)}$. The unstable equilibrium data obey EF diffusion. However, Stable bubbles along the island boundary exhibit dramatically lower values, falling while traversing the lower segment. Strikingly, the upper segment yields a constant (0.0018) value. This is consistent with the fact that both R_{max} and R_0 are increasing, and their opposite effects on the dynamic mass flux just balance each other. We cannot explain this result, although it can be interpreted as a decrease in the effective gas concentration just outside the bubble. Differential (or preferential) diffusion may play a role here. Whatever the mass stabilization mechanism is, we can now quantify its constraint on values of (P_a, R_0) on the upper island boundary: $C_i/C_{0\,(eq.(1))}$ is a constant of the motion.

Conclusion]

We have observed mechanical stability and mass transport boundaries in the parameter space of an acoustically levitated bubble which determine its behavior. The Faraday instability limits the maximum equilibrium size of spherically oscillating bubbles at a fixed pressure, while dynamic mass flux equilibrium constrains the size of a bubble at fixed pressure such that it remains along a stable, zero-mass-flux path. This constraint yields very high values of bubble response, and thus provides a window in state space in which S11S1. appears. The key observation is the existence of tbc dissolution island (which stabilizes spherical oscillations relative to the Faraday instability) and its dependence on the dissolved gas concentration.

The research described in this paper was carried out at the Jet Propulsion Laboratory, California Institute of Technology, under contract with the National Aeronautics and Space Administration. Wc gratefully acknowledge the usc of equipment loaned to us by E. Trinh.

Footnotes

1. Plesset, M.S. and S.A. Zwick, J. Appl. Phys. 23, 95 (1952); Yasui, K., J. Acoust. Soc. Am. **98**, 2772 (1995).

2. Eller, A. and H.G. Flynn, J. Acoust. Soc. Am. 37, 493 (1965); Gould, R. K., J. Acoust. Soc. Am. 56, 1740 (1974); Church, C.C., J. Acoust. Soc. Am. **83**, 2210 (1988); Fyrillas, M.M. and A.J. Szeri, J. Fluid. Mech. *277*, 381 (1994); Löfstedt, R. et al., Phys. Rev. E **51**, 44(10 (1995); Brenner, M.P. et al., Phys. Rev. Lett. 76, 1158 (1996).

3. Crum, L. A., J. Acoust. Soc. Am. **68**, 203 (1980); Johnson, D.O. and K.J. Stebe, J. Colloid Interface Sci. **168**, 21 (1994); Fyrillas, M.M. and A.J. Szeri, J. Fluid. Mech. 289, 295 (1995).

4. Hickling, R. and M.S. Plesset, Phys. Fluids 7, 7 (1964); Wu, C.C. and P.H. Roberts, Phys. Rev. Lett. 70, 3424 (1993).

5. Holt, R. G., J. Holzfuss, A. Judt, A. Phillip, and S. Horsburgh, *Proceedings of the 12th International Symposium on Nonlinear Acoustics, Austin, Texas*, M.F. Hamilton and D.T. Blackstock, eds., (Elsevier, New York, 1990), p. 497; Holt, R. G., D.F. Gaitan, A.A. Atchley and J. Holzfuss, Phys. Rev. Lett. 72, 1376 (1994).

6. Birkhoff, G., Q. Appl. Mech. **12**, 306 (1954); **13**, 451 (1956); Eller, A. I. and L. A. Crum, J. Acoust. Soc. Am. 47, 762 (1970); Strube, H. W., Acustica 25, 289 (1971); Hullin, C., Acustica 37, 64 (1977); Brenner, M.P. et al., Phys. Rev. Lett. 75, 954 (1995).

7. Marinesco, N. and J.J. Trillat, Proc. R. Acad. Sci. **196**, 858 (1933); Gaitan, D.F. et al., J. Acoust. Soc. Am. **91**, 3166 (1992); Barber, B. P. and S.J. Putterman, Nature 352, 318 (1991); Barber, B.P. et al., Phys. Rev. Lett. 74, 5276 (1995).

8. There is rough agreement among various groups, and the differences are due in the main to 1) different acoustic frequencies; and 2) the methods utilized for either inferring P_a and R_0 from light scattering (Barber, B.P. et al., Phys. Rev. Lett. 72, 1380 (1994); Löfstedt R. et al. in [2]) or calibrating P_a and R_0 measurements (this work; Gaitan, D.F., PhD thesis, Univ. Mississippi, (1990; Cordry, S. M., PhD thesis, Univ. Mississippi, (1995); Stottlemyer, T.K., PhD thesis, Yale Univ., (1996)).

9. Faraday, M. Phil. Trans. Royal Soc. London 121, 299 (1 831).

10. This source of 'dancing' translations (often noted by the UCLA group, see Barber et al. and Löfstedt et al in [8] and Weninger, K. et al., J. Phys. Chem. **99**, 14195 (1995)) should be distinguished from another shape-oscillation phenomenon, namely, self-propulsion due to coupling between shape modes (see Eller and Crum in [6]; Benjamin, 'T'. Brooke and Albert 'T'. Ellis, J. Fluid Mech. 212, 65 (1990); Feng, Z.C. and L.G. Leal, Phys. Fluids 7, 1325 (1995).

11. As did Gaitan et al. in [7], their Figs. 20 and 21; and later Barber et al. in [7], their Fig. 4.

12. Fig. 2 in Barber et al. in [8]; Figs. 1, 8, 11 and 12 in Löfstedt et al. in [2], where different combinations of gas are used, but always at total gas partial pressure near 150 "Torr, thus in the range 0.1 $\leq C_i/C_0 \leq$ 0.5. This leads us to believe that the dissolution island is a generic feature, and thus highly dependent on gas solubility, but only weakly dependent on the thermodynamic equation of state of the particular gas.

13. Taylor, G.I., Proc. Royal Soc. A 201, 192 (1950).

14. Holt, R.G. and L.A. Crum, J. Acoust. Soc. Am. 91, 1924 (1 992).

15. Holt, R.G. and L.A. Crum, Appl. Opt. *29, 4182* (1990).

16. Holt, R.G. and D.F. Gaitan, APS Bulletin 40, 1960 (1995).

17. Lamb, H., *Hydrodynamics* (Dover, New York, 1945).

18. Prosperetti, A., L.A. Crum, K.W. Commander, J. Acoust. Sot. Am. **83**, 502 (1988). The curves EF were computed using an incompressible, polytropic model with lumped element damping; we used the version found in Prosperetti et al. to check our results: they were the same over the parameters reported.

19. Parlitz, U., V. Englisch, C. Scheffczyk, and W. Lauterborn, J. Acoust. Soc. Am. **88**, 1061 (1990); Church, C.C. in [2].

R_0 at Unstable equilibrium (μm)	7.5 ± 1.0	23.1± 1.()	18.0 ± 1.5	9.9 ± 1.5	14.8 ± 1.5
C_i/C_0 *(meas.)* (Henry's law)	().()8 ± 0.03	0.66 ± ().()3	0.5 ± ().()6	0.16 ± ().()7	0.46 ± 0,1
C_i/C_0 *(eq. (1))* (measured $R(t)$)	().()84 ± 0.02	**0.60** ± ().()2	**().44** ± ().()3	0.18 ± ().()3	0.30 ± 0.03

Table 1

Comparison of dissolved gas concentration $C_i/C_{0\,(meas.)}$ (using Henry's law for the degassing of the water prior starting an experimental run) with $C_i/C_{0\,(eq.\,(1))}$, calculated from Eq. (1) using our $R(t)$ measured from light scattering. Also given is the corresponding measured equilibrium bubble size at the EF-F intersection.

Figure Captions

1. Surfaces of constant dissolved air concentration from the 3-D state space $(P_a, R_0, C_i/C_0)$ for acoustically levitated air bubbles in pure water. All bubbles are levitated in a cylindrical cell at 20.6 kHz. The symbols labeled 'F n' are the measured values (P_a, R_0) at the onset of the Faraday instability for the nth mode ('?' indicates mode was undetermined). The line labeled '1 3F (C_i/C_0)' is the numerically generated diffusional equilibrium (1) for the experimentally measured C_i/C_0 *(meas.)* using an RP equation I 1 8]. The solid points are the measured mass flux equilibria at the given **concentration:** squares are stable, inverted triangles are unstable. Bubbles are observed to grow in regions labeled 'g'; to dissolve in dark shaded regions labeled 'd'. (a) $C_i/C_0 \approx 0.5$; (b) $C_i/C_0 \approx 0.45$; (c) $C_i/C_0 \approx 0.2$; the mow labeled 'S1 .' indicates the minimum (P_a, R_0) where light is first emitted.

2. Dissolved gas concentration $C_i/C_{0\,(eq.\,(1))}$ calculated from (1) using the measured $R(t)$ for tile stable and unstable miss flux equilibria vs acoustic pressure P_a for two data sets. The measured $C_i/C_{0\,(meas.)}$ from Henry's law is constant for each data set and drawn **on** the **axis; only the** unstable equilibria are in diffusive equilibrium.

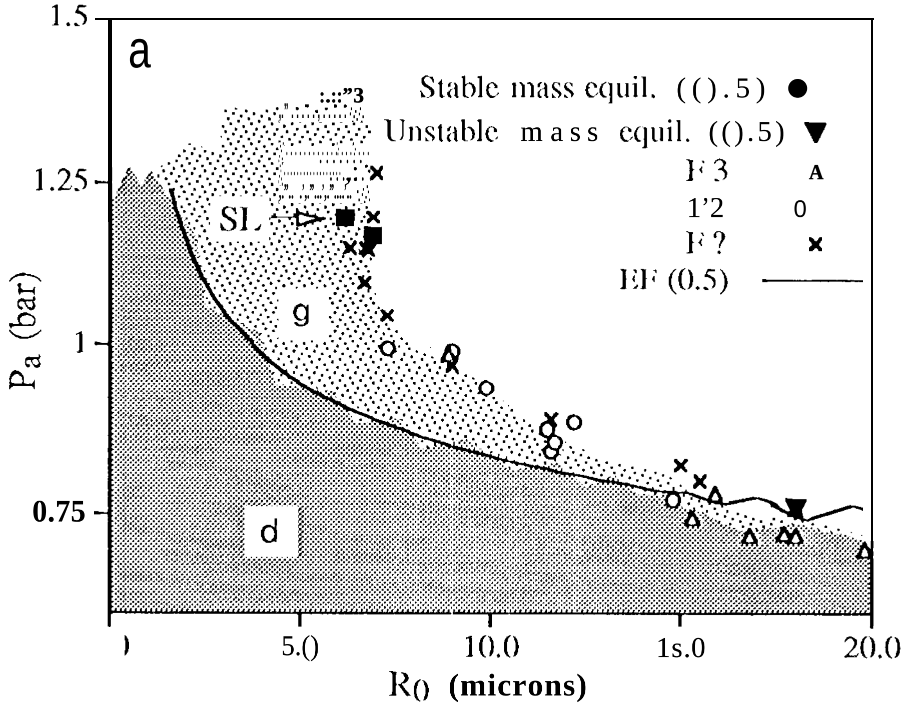

a
Stable mass equil. (().5)
Unstable mass equil. (().5)
F3
1'2
F?
EF (0.5)
SL
g
d
1.5
1.25
1
0.75
Pa (bar)
5.()
10.0
1s.0
20.0
R() (microns)

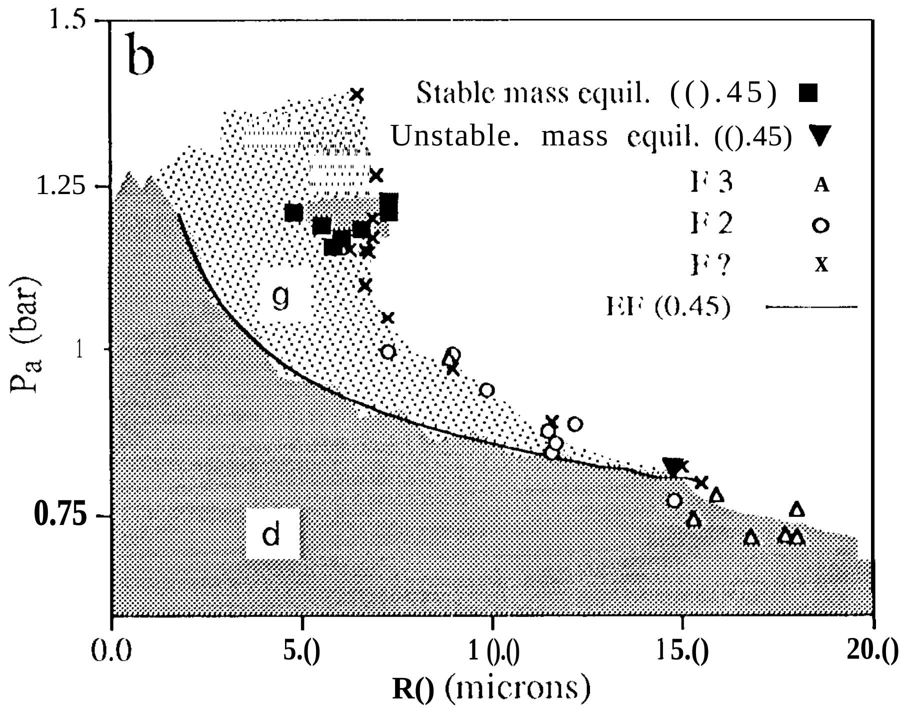

b
Stable mass equil. (().45)
Unstable. mass equil. (().45)
F 3
F 2
F ?
EF (0.45)
g
d
1.5
1.25
1
0.75
Pa (bar)
0.0
5.()
1 ().()
15.()
20.()
R() (microns)

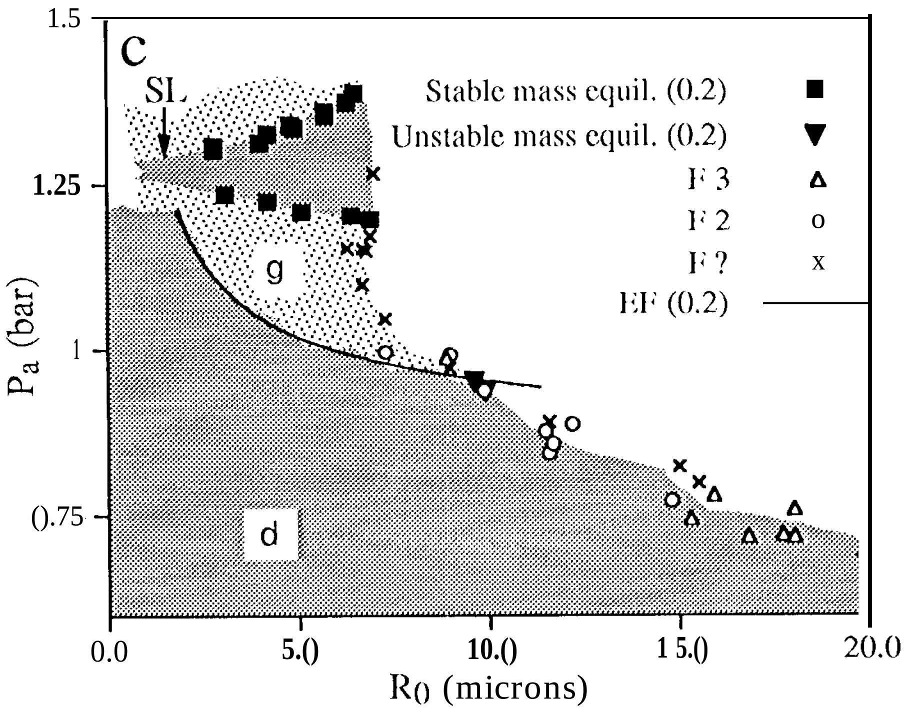

C
SL
Stable mass equil. (0.2)
Unstable mass equil. (0.2)
F 3
F 2
F ?
EF (0.2)
g
d
1.5
1.25
1
0.75
Pa (bar)
0.0
5.0
10.0
15.0
20.0
R0 (microns)

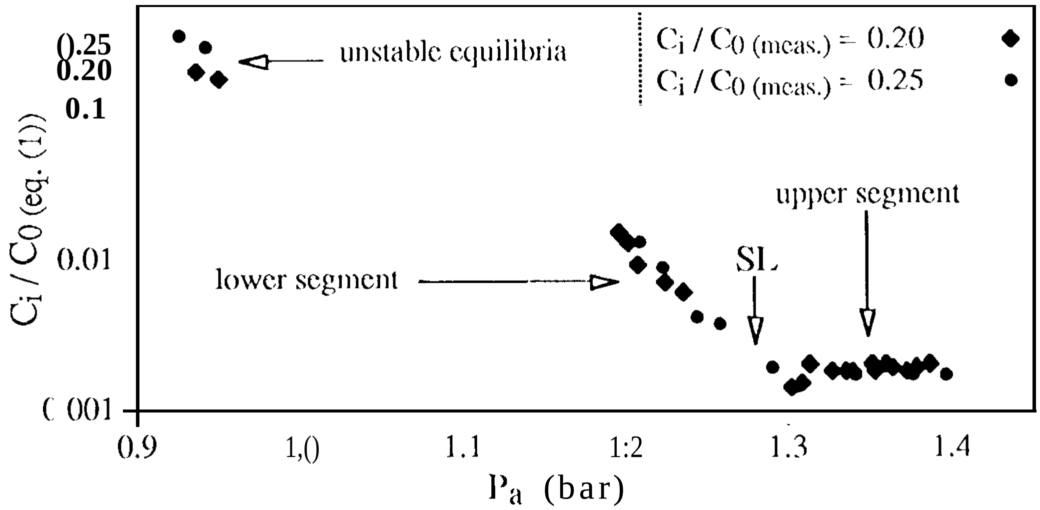

0.25
0.20
0.1
0.01
0.001
unstable equilibria
Ci / C0 (meas.) = 0.20
Ci / C0 (meas.) = 0.25
upper segment
lower segment
SL
Ci / C0 (eq. (1))
0.9
1.0
1.1
1.2
1.3
1.4
Pa (bar)